

## Fracture toughness of high performance concrete subjected to elevated temperatures Part 1 The effects of heating temperatures and testing conditions (hot and cold)

Binsheng Zhang<sup>\*</sup>, Martin Cullen<sup>a</sup> and Tony Kilpatrick<sup>b</sup>

*School of Engineering and Built Environment, Glasgow Caledonian University,  
Glasgow G4 0BA, Scotland, United Kingdom*

*(Received November 25, 2013, Revised June 15, 2014, Accepted June 20, 2014)*

**Abstract.** In this study, the fracture toughness  $K_{IC}$  of high performance concrete (HPC) was determined by conducting three-point bending tests on eighty notched HPC beams of 500 mm × 100 mm × 100 mm at high temperatures up to 450°C (hot) and in cooled-down states (cold). When the concrete beams exposed to high temperatures for 16 hours, both thermal and hygric equilibriums were generally achieved.  $K_{IC}$  for the hot concrete sustained a monotonic decrease tendency with the increasing temperature, with a sudden drop at 105°C. For the cold concrete,  $K_{IC}$  sustained a two-stage decrease trend, dropping slowly with the heating temperature up to 150°C and rapidly thereafter. The fracture energy-based fracture toughness  $K_{IC}'$  was found to follow similar decrease trends with the heating temperature. The weight loss, the fracture energy and the modulus of rupture were also evaluated.

**Keywords:** high performance concrete; high temperature; fracture toughness; test conditions

---

### 1. Introduction

In modern concrete constructions, e.g. tall reinforced concrete buildings, reinforced concrete cooling towers in thermal power plants, prestressed concrete pressure vessels in nuclear power stations, prestressed concrete silos in chemical factories, long prestressed concrete bridges, etc., high strength and even ultra-high strength concrete has been largely used but the concrete needs to have ability to resist elevated temperatures. A higher concrete strength normally leads to a higher toughness but also dramatically to a lower brittleness, which unavoidably causes concrete to fail very suddenly and even explosively. The information about fundamental properties such as strength, stiffness, toughness and brittleness under highly elevated temperatures is very often required. Besides strength and stiffness, the fracture toughness is a very useful fracture parameter for manufacturing high strength high performance concrete materials, designing modern concrete structures, conducting structural analysis and simulations under various loading and environmental

---

<sup>\*</sup>Corresponding author, Senior Lecturer, Ph.D., E-mail: Ben.Zhang@gcu.ac.uk

<sup>a</sup>Senior Lecturer, E-mail: M.N.Cullen@gcu.ac.uk

<sup>b</sup>Senior Lecturer, E-mail: A.R.Kilpatrick@gcu.ac.uk

conditions, and assessing post-fire safety of reinforced and prestressed high strength concrete structures. Many investigations have been carried out into the fracture toughness of high performance concrete at room temperature, but the information about its performance at high temperatures is still limited. Extensive research into fracture properties of concrete at high temperatures only started about four decades ago and much progress has since been made (RILEM 1985, Schneider 1988, Bažant and Kaplan 1996, Phan and Carino 1998, Zhang *et al.* 2000a, 2000b, 2000c, Cülfik and Özturan 2002, Peng *et al.* 2006, Zhang and Bićanić 2006, Kanellopoulos *et al.* 2009, Ulm and James 2011, Watanabe *et al.* 2013).

High temperature influences the behaviour of concrete at different structural levels. At micro and meso levels, concrete sustains physical and chemical changes. Physically, thermal dilations, thermal shrinkage and creep associated with water loss normally lead to large volume changes which can result in large internal stresses and strains such as interfacial thermal incompatibility and lead to micro cracking and fractures. Heating temperature also changes pore structures (porosity and pore size distribution) (Yan *et al.* 2000). High temperatures cause thermal and hygric gradients which lead to migration of water (diffusion, drying). Especially for high strength high performance concrete with smaller pore sizes, rapid exposure to high temperatures can cause high pore pressures and lead to explosive spalling, which will be potentially disastrous (Bangi and Horiguchi 2011, Zhang *et al.* 2013). High temperatures also cause chemical and micro-structural changes, such as migration of water (diffusion, drying), increased dehydration, interfacial thermal incompatibility and chemical decomposition of hardened cement paste and aggregates. In general, exposure to high temperatures, the mechanical and structural characteristics of high performance concrete including strength, stiffness and toughness will be largely degraded.

Strength, stiffness, toughness and brittleness are all fundamental fracture properties for assessing the resistance of high performance concrete against cracking and fracture. Toughness commonly characterises the capacity of concrete to resist deformation and fracture so it is a synthetic property. By contrast, brittleness is commonly understood to be the tendency for concrete to fracture rapidly before significant deformation occurs. Nowadays super high strength high performance concrete with compressive strength over 250 MPa or even up to 300 MPa has been manufactured and applied into practical concrete construction (Nielson 1995, Haghighi *et al.* 2007, Pu 2012). To date, much research has been conducted on the strength and stiffness of high performance concrete at varied heating scenarios (Felicetti and Gambarova 1998, Abe *et al.* 1999, Zhang *et al.* 2000a, Zhang and Bićanić 2002a, 2006, Chen and Liu 2004, Peng *et al.* 2006, Watanabe *et al.* 2013), and has indicated that the strength and stiffness of concrete decreased with increasing heating temperature, exposure time and thermal cycles. Some research has also been done on the toughness of high performance concrete (Zhang *et al.* 2000b, 2000c, Nielson and Bićanić 2003, Zhang and Bićanić 2006, Kanellopoulos *et al.* 2009, Watanabe *et al.* 2013, Yu and Lu 2013). As for the brittleness of high performance concrete at high temperatures, not much information is available. The characteristic length  $l_{ch}$  proposed by Hillerborg (Hillerborg *et al.* 1976) was used to assess the brittleness of normal- and high-strength concrete and was found to increase with the increasing heating temperature and exposure time, which indicates that the concrete brittleness monotonically decreased with the increasing heating temperature and heating time (Zhang *et al.* 2000a). The ratio of the plastic and/or total energy/deformation to the elastic energy/deformation used as toughness indexes was also proposed to quantitatively assess the concrete brittleness and similar conclusions were drawn (Zhang *et al.* 2000b, 2000c, 2002b).

Two parameters have generally been used to assess the toughness of concrete, i.e. the fracture energy  $G_F$  and the fracture toughness  $K_{IC}$ , and they both increased with the increasing strength at

room temperature. At high temperatures,  $G_F$  first increased with heating temperature until a transition point was reached and then gradually decreased (Bažant and Prat 1988, Baker 1996, Zhang *et al.* 2000a). The temperature corresponding to this point was found to be 300°C for siliceous gravel concrete (Zhang and Bićanić 2002a) and basalt dolerite concrete (Zhang and Bićanić 2006). A temperature of 450°C for this transient point was also reported when the concrete was heated to 600°C (Yu and Lu 2013). Prokoski (Prokoski 1995) may be the earliest researcher who measured the fracture toughness of ordinary and refractory concretes exposed up to 1300°C at 28 days on the concrete beams under three-point bending. He found the fracture toughness for Mode I,  $K_{IC}$ , continuously decreased with the increasing heating temperatures from 0.643 MN/m<sup>1.5</sup> at 20°C to 0.044 MN/m<sup>1.5</sup> at 1100°C for the ordinary concrete and from 0.718 MN/m<sup>1.5</sup> to 0.343 MN/m<sup>1.5</sup> at 1300°C for the refractory concrete. However, an exposure time of 2 hours at high temperatures might not be long enough to obtain a uniform temperature within the concrete specimen and very large thermal and hygric gradients would still exist. In his calculations, he only used the initial crack length and ignored the propagation of the pre-crack, which led to the values of  $K_{IC}$  to be geometrically dependent. Hamoush (Hamoush *et al.* 1998) measured the residual fracture toughness of normal strength crushed limestone concrete on forty-five edge-notched beams under three-point bending by considering a process zone (crack extension zone) at the peak load and found that  $K_{IC}$  monotonically decreased with increasing temperatures. The maximum heating temperature in his study was only 300°C so the application of his test results is limited. Meanwhile, neither of them considered the effect of self-weight of the beam even though this effect became more significant with the increasing heating temperature. This would lead to his test data to be less accurate. Zhang *et al.* (2002a) investigated the classic fracture toughness,  $K_{IC}$ , and the fracture energy related fracture toughness,  $K_{IC}'$ , for assessing the residual fracture toughness of heated normal- and high-strength concrete.  $K_{IC}$  is an instantaneous parameter that represents the crack resistance of concrete at the peak load, while  $K_{IC}'$  is a synthetic process parameter that represents the crack resistance over the whole failure process. The effects of heating temperature, exposure time and curing age on the fracture toughness were experimentally investigated and analysed by conducting three-point bending tests on eighty-seven notched normal- and high-strength concrete beams that had been heated between 100°C and 600°C. Various exposure times up to 168 hours and cooled down to the room temperature. Four testing ages from 7 to 90 days were adopted. Higher heating temperature over 200°C generally decreased fracture toughness but below 200°C some strengthening and toughening effect was observed. Similar phenomenon was found for longer exposure time as well but such effect was more significant at the early exposure stage under 12 hours. Longer curing age only led to slightly larger toughness in the first 28 days and became little influential thereafter. Weight loss was also measured to distinguish different stages of the fracture toughness of concrete with heating temperatures. The quick evaporation of capillary water hardly affected the fracture toughness but the evaporation of gel water and chemically bound water and the decomposition significantly decreased the fracture toughness.

So far, information about the fracture toughness of concrete exposed to high temperatures is very limited even though  $K_{IC}$  can be used to assess the resistance of concrete against cracking and failure at high temperatures. The determination of the fracture process zone size will be very important for accurately calculating the fracture toughness at high temperatures. Hence, more work needs to be done to further study the effect of varied heating scenarios on the fracture toughness of concrete at high temperatures. The effect of moisture migration on the fracture toughness also needs to be further investigated.

In this study, the whole test programme was divided into several series. Each series was specially designed to target one parameter which would largely influence the fracture toughness and other fracture properties of high performance concrete. These included the heating temperature  $T_m$ , the testing conditions (hot and cold), the heating rate, the cooling rate (cooling methods) and the exposure time at the designated temperature. In this paper, the test results regarding the effects of the heating temperature  $T_m$  and the testing conditions (hot or cold) on the fracture toughness and other properties of the concrete are presented. Those effects were investigated by conducting three-point bending tests on the notched beams of high performance concrete in a furnace. Beside the fracture toughness  $K_{IC}$  as a primary parameter, the compressive strength  $f_{cu}$ , the splitting tensile strength  $f_t'$ , the modulus of rupture  $f_r$ , the fracture toughness  $G_F$  and the Young's modulus  $E$  were also studied.  $K_{IC}$ ,  $G_F$  and  $f_r$  were measured under both hot and cold conditions, whereas other properties were measured after cooling (residual). The weight loss  $\omega$  was continuously measured while the concrete was heated and could be used to further study its effect on the fracture behaviour of the concrete during heating. Thus, the relationships of  $K_{IC}$  and other properties with  $T_m$ , the testing conditions (hot and cold) and  $\omega$  could be established.

## 2. Fracture mechanics and fracture toughness

### 2.1 Application of fracture mechanics to concrete

Since Kaplan first measured the fracture toughness and strain energy release rate of concrete in the early 1960s (Kaplan 1961), much theoretical and experimental work has been done to assess whether linear elastic fracture mechanics (LEFM) could be directly applied to concrete materials. Concrete is neither a perfect elastic brittle material like glass nor a quasi-brittle material and shows some non-linearity before the peak load is reached. Accordingly the stable crack growth, also termed as the fracture process zone, occurs due to micro cracks in the mortar and bond cracks at the cement paste-aggregate interface, or crack arresting, kinking and linking between aggregate particles, or a macro crack. All of this makes the measured fracture toughness become geometrically dependent. To accurately determine the fracture toughness of concrete, the stable crack growth has to be added to the initial notch depth and the effective crack length is adopted. Thus, the obtained fracture toughness as a true material property will be fully geometrically independent. Hillerborg used the fictitious crack model to determine fracture energy (Hillerborg *et al.* 1976). Bažant *et al.* used the size effect model and the crack band model to determine  $R$ -curve parameters, fracture energy, crack band width, strain softening modulus, etc. (Bažant and Oh 1983, Bažant 1984, Bažant *et al.* 1986, Gettu *et al.* 1990). Karihaloo and Nallathambi extensively investigated the effects of crack size, water/cement ratio and coarse aggregate texture on the fracture toughness of concrete and proposed the effective crack model based on massive test data for calculating the fracture toughness, and their empirical formulae are very convenient to use (Nallathambi *et al.* 1984, Karihaloo and Nallathambi 1989). Shah proposed the two-parameter fracture model to work out the effective crack length so as to eliminate the effect of geometry (Shah 1990). A parameter with length dimension was also used to determine the maximum load, notch sensitivity,  $R$ -curve, etc. RILEM (RILEM 1990a, 1990b) proposed the drafts for determining the fracture toughness  $K_{IC}$  and the critical crack tip opening displacement  $CTOD_c$  by using either Shah's two-parameter model (Shah 1990) or Bažant's size effect model (Bažant *et al.* 1986). Guinea, Planas and Elices (Guinea *et al.* 1992, Planas *et al.* 1992, Elices *et al.* 1992) identified

possible sources of the experimental error in the RILEM method (RILEM 1985) for measuring the fracture energy and proposed a method to eliminate the major source of the error by including the work-of-fracture due to practical difficulties in capturing the tail part on the load-deflection curve. Their model was later applied and developed further (Rosselló and Elices 2004, Rosselló *et al.* 2006). Direct tension (Phillips and Zhang 1993) and splitting tension tests (Ince 2010) were tried to obtain stable fracture toughness of concrete. Xu and Reinhardt proposed the double- $K$  fracture model to simulate the fracture of concrete including the initial fracture toughness  $K_{IC}^{ini}$  and the unstable fracture toughness  $K_{IC}^{un}$  (Xu and Reinhardt 1999a, 1999b, 1999c, 2000). These two fracture toughness parameters were obtained from the initial fracture energy release rate  $G_{IC}^{ini}$  and the unstable fracture energy release rate  $G_{IC}^{un}$  measured on compact tension, wedge splitting and three-point bending concrete specimens. Zhao, Kwon and Shah investigated the effect of specimen size on the fracture energy and softening curve of concrete using inverse analysis on the test data (Zhao *et al.* 2008, Kwon *et al.* 2008). Very recently, Murthy and Karihaloo extensively investigated the size effect on the specific fracture energy of normal- and high-strength concrete using tri-linear and other methods (Karihaloo *et al.* 2013, Murphy *et al.* 2013).

## 2.2 Fracture toughness of concrete

In the linear fracture mechanics (*LEFM*), the fracture toughness for mode I,  $K_{IC}$ , also called the critical stress intensity factor, is generally calculated from

$$K_{IC} = \sigma_N \sqrt{a} F(\alpha) \quad (1)$$

where

- $\sigma_N$  is the nominal applied stress,
- $a$  is the effective crack length,  $a = a_0 + \Delta a$ ,
- $a_0$  is the initial notch depth,
- $\Delta a$  is the crack propagation at peak load and is also widely regarded as the size of the process zone or crack zone,
- $\alpha$  is the effective notch-depth ratio and  $\alpha = a/H$ ,
- $H$  is the specimen depth,
- $F(\alpha)$  is a geometric function.

Different test methods can be used to determine  $K_{IC}$  and the three-point bending test on a single-edge notched beam is the most popular one. Fig. 1 shows the arrangement of the three-point bending test on a notched concrete beam. Thus,  $\sigma_N$  in Eq. (1) is equal to the modulus of rupture of the corresponding un-notched beam and can be expressed by considering the self-weight of the beam as

$$\sigma_N = \frac{6M}{BH^2} = \frac{1.5(P_u + P_0)S}{BH^2} = \frac{1.5[P_u + 0.5mg(L/S)(2-L/S)]S}{BH^2} \quad (2)$$

where

- $B$  is the width of the beam,
- $L$  is the full length of the beam,

$S$  is the effective span,  
 $M$  is the maximum moment at the middle span, given by  $M = (P_u + P_0)S/4$ ,  
 $P_u$  is the maximum load at peak,  
 $P_0$  is the equivalent load due to the self-weight of the beam and  
 $P_0 = 0.5 m g (L/S) (2 - L/S)$ ,  
 $m$  is the mass of the beam between the supports and is calculated as  $m = m_0 (S / L)$ ,  
 $m_0$  is the total mass of the beam,  
 $g$  is the acceleration due to gravity and  $g = 9.81 \text{ m/s}^2$ .

Here, the factor  $(L/S)(2 - L/S)$  is used to eliminate the influence of the cantilever parts of the concrete beam outside the supports.

Here the ligament height  $h$  is equal to  $H - a$ . At high temperatures, the self-weight of the beam will no longer be constant but very much depend on the heating scenario. Hence  $m$  should be replaced by the actual mass  $m'$  which is defined as

$$m' = m(1 - \omega) \quad (3)$$

where  $\omega$  is the percentage weight loss during heating, greatly dependent on heating scenarios. For  $S/H = 4$ , the geometric function  $F(\alpha)$  can be expressed as (Karihaloo and Nallathambi 1989, RILEM 1990a)

$$F(\alpha) = \frac{1.99 - \alpha(1 - \alpha)(2.15 - 3.93\alpha + 2.70\alpha^2)}{(1 + 2\alpha)(1 - \alpha)^{3/2}} \quad (4)$$

Different models have been proposed to calculate the effective crack length  $a$ , including Bažant's size effect model (Bažant *et al.* 1986), Shah's two parameter model (Shah 1990), Karihaloo's empirical model (Nallathambi *et al.* 1984, Karihaloo and Nallathambi 1989), etc. All these models can give very close results. In Bažant's model,  $a$  cannot be directly obtained and a series of tests need to be conducted to determine the parameters. In Shah's model, sometimes a servo test machine has to be used to obtain a stable load-displacement curve and carry out unloading at or soon after the peak load to obtain the instantaneous compliance. However, Karihaloo's model is more simple and direct so it is adopted in this study. From this model, the effective crack length  $a$  can be obtained from

$$\frac{a}{H} = \gamma_1 \left( \frac{\sigma_N}{E} \right)^{\gamma_2} \left( \frac{a_0}{H} \right)^{\gamma_3} \left( 1 + \frac{d}{H} \right)^{\gamma_4} \quad (5)$$

where

$d$  is the maximum aggregate size used in the concrete mix,

$E$  is the Young's modulus of concrete,

$\gamma_1$  to  $\gamma_4$  are constants and can be obtained from the best fit of test data.

When  $E$  is obtained from separate tests,  $\gamma_1 = 0.198$ ,  $\gamma_2 = -0.131$ ,  $\gamma_3 = 0.394$  and  $\gamma_4 = 0.600$  (Karihaloo and Nallathambi 1989). In this model, the material role is governed by the elastic deformability  $\sigma_N/E$  and the texture heterogeneity through the aggregate size  $d$ . The latter is likely to be affected by thermal damage as well. Here, the effect of heating temperature is only considered in the  $\sigma_N/E$  ratio.

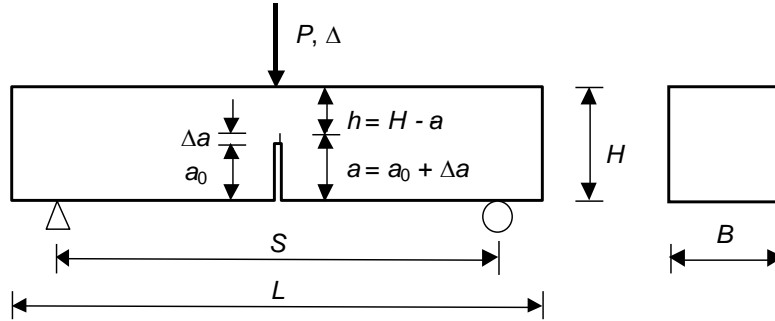


Fig. 1 Dimensions of a single edge notched beam in three-point bending

In the process for determining  $K_{IC}$ ,  $\sigma_N$  is first calculate using Eq. (2), then followed by determining  $\alpha = a/H$  using Eq. (5) and  $F(\alpha)$  using Eq. (4), and finally calculating  $K_{IC}$  using Eq. (1). The modulus of rupture  $f_r$  of the notched beam can be determined as

$$f_r = \frac{6M}{B(H-a_0)^2} = \frac{1.5(P_u + P_0)S}{B(H-a_0)^2} = \frac{1.5[P_u + 0.5mg(L/S)(2-L/S)]S}{B(H-a_0)^2} \quad (6)$$

In this study,  $a_0/H = 0.5$  so  $f_r = 4\sigma_N$ .

The fracture energy,  $G_F$ , defined as the total energy dissipated over a unit area of the cracked ligament, was obtained on the basis of the work done by the force (the area under a load-displacement curve ( $P - \Delta$  curve) in three-point bending on a centrally notched beam) associated with the gravitational work done by the self-weight of the beam.  $G_F$  was calculated based on the following formula:

$$G_F = \frac{\int_0^{\Delta_0} P(\Delta) d\Delta + m'g(L/S)(2-L/S)\Delta_0}{B(H-a_0)} \quad (7)$$

Here,  $\Delta_0$  is the ultimate displacement when the beam is broken.

The fracture toughness can also be calculated using the fracture energy  $G_F$  and the Young's modulus  $E$  in LEFM, termed as  $K_{IC}'$  to distinguish from the classic fracture toughness  $K_{IC}$ , as follows

$$K_{IC}' = \sqrt{G_F E} \quad (8)$$

The classic fracture toughness  $K_{IC}$  is obtained based on the ultimate load on the ascending branch of a load-displacement curve, including linear loading and hardening. It can be used to reflect the resistance of concrete against cracking. However, it cannot represent the crack resistance of the heated concrete over the whole loading process because it neglects the resistance after the peak load, i.e. softening property. In other words, the crack resistance of concrete can be represented using load capacity and deformation ability, i.e. energy dissipation. This resistance can be well reflected using the fracture energy  $G_F$ . If the stiffness change is included, the fracture toughness of concrete exposed to high temperatures can be more reasonably described. Thus, the

fracture toughness related to fracture energy,  $K_{IC}'$ , can play this important role. Because  $K_{IC}'$  can represent the behaviour of concrete at both ascending and descending branches of the complete loading process including linear, hardening and softening, its magnitude can be expected to be larger than  $K_{IC}$  but its physical meaning can be clearer and more reasonable.

### 3. Experimental

#### 3.1 Concrete specimens

Eight heating temperatures were adopted as  $T_m = 105^\circ\text{C}$ ,  $150^\circ\text{C}$ ,  $200^\circ\text{C}$ ,  $250^\circ\text{C}$ ,  $300^\circ\text{C}$ ,  $350^\circ\text{C}$ ,  $400^\circ\text{C}$  and  $450^\circ\text{C}$ , respectively, with a constant heating rate of  $\dot{T}^+ = 3^\circ\text{C}/\text{min}$  for a fixed exposure 16 hours. Cooling was achieved by leaving the furnace fully closed to obtain slow cooling conditions. A total of eighty beams were tested with at least three beams for each scenario, and prisms were tested for measuring the residual Young's modulus. As bench marks, five beams and three prisms were tested at  $20^\circ\text{C}$ . Table 1 lists the arrangement of this test series.

The primary fracture parameters measured under both hot and cold conditions were the fracture toughness  $K_{IC}$ , the fracture energy  $G_F$  and the modulus of rupture  $f_r$ . The residual material properties measured were the compressive strength  $f_{cu}$ , the splitting tensile strength  $f_t'$ , the Young's modulus  $E$  and the concrete density  $\rho$ . The weight loss  $\omega$  was continuously measured while the concrete was being heated. Part of the test data for the above mentioned parameters for different heating scenarios have been reported in the previous publications (Zhang and Bićanić 2006, Zhang 2011, Zhang *et al.* 2013).

Table 1 Arrangement of the test series

Heating rate $\dot{T}^+$ ( $^\circ\text{C}/\text{min}$ )	Heating temperature $T_m$ ( $^\circ\text{C}$ )	Exposure time $t_h$ (hour)	Number of beam specimens	Properties at high temperature	Residual properties
/	20	/	5	$G_F, f_r, K_{IC}, K_{IC}', f_{cu}, f_t', E, \rho$	
3	105	16	7 (4 + 3)	$G_F, f_r, K_{IC},$ $K_{IC}', \rho, \omega$	$G_F, f_r, K_{IC},$ $K_{IC}', f_{cu}, f_t',$ $E, \rho, \omega$
	150		10 (7 + 3)		
	200		10 (7 + 3)		
	250		10 (7 + 3)		
	300		10 (7 + 3)		
	350		10 (7 + 3)		
	400		9 (6 + 3)		
	450		9 (6 + 3)		
Total			80		

Table 2 Concrete mix design

Ingredient	OPC	PFA	Quartz sand	10 mm dolerite	20 mm dolerite	Water	Plasticiser
Weight ratio	1	0.33	2.45	1.39	2.78	0.56	0.006
Quantities ( $\text{kg}/\text{m}^3$ )	300	99	735	417	834	168	1.8

Notched concrete beams of 500 mm × 100 mm × 100 mm, with a 400 mm effective span and a 50 mm notch depth, were loaded under three-point bending for determining  $G_F$ ,  $K_{IC}$  and  $f_r$ . Notches were prepared using a diamond saw before being heated. Concrete prisms of 200 mm × 100 mm × 100 mm were cast for determining the residual  $E$ , three for each scenario. To effectively utilise the heated concrete, 100 mm cubes were cut from the broken beams for determining  $f_{cu}$  and  $f'_t$ .

The 42.5N OPC and PFA were adopted as adhesive materials. The aggregates included calcareous quartz sand, 10 mm single-sized and 20 mm graded quartz dolerites. Pozzoloth 300 N plasticiser was used to achieve a slump of 125 mm. The concrete mix design is listed in Table 2. The test age was at least 90 days to allow full hydration, giving  $f_r = 6.35$  MPa,  $f_{cu} = 67.1$  MPa,  $f'_t = 4.47$  MPa,  $E = 35.6$  GPa,  $\rho = 2463$  kg/m<sup>3</sup>,  $G_F = 228.2$  N/m,  $K_{IC} = 1.389$  MN/m<sup>1.5</sup> and  $K_{IC}' = 2.845$  MN/m<sup>1.5</sup>.

### 3.2 Heating furnace and testing facility

A program-controlled three-zone VTS furnace ( $600 \pm 5^\circ\text{C}$ ) was specially designed and it had two identical halves with an inner dimension of 600 mm × 600 mm × 800 mm. Fans were used to circulate the air in the furnace for heating the concrete uniformly and cooling the loading pieces. The furnace was built within a 2000 kN LOS universal testing machine to allow the tests to be conducted at high temperatures. Fig. 2 shows the furnace with the testing machine.

A high yield strength steel loading piece, including bottom block and top plate, was designed to allow two beams to be tested while being hot in one heating batch. The bottom block was connected to the lower actuator of the machine. The top plate could slide against the block after it was slightly raised by using two lifting bars. Prior to heating, two beams were put on the loading piece symmetrically in the furnace. When the heating process was completed, one beam was lifted to the centre of the machine and then tested. The second beam could then be lifted to the centre for testing. High yield strength steel was also used for the top piece which was connected to the upper actuator. According to the requirement by RILEM (1985), a roller bearing was used for one support for each beam and a ball bearing for the other. Fig. 3 illustrates the top and bottom loading pieces with the twin concrete specimens.



Fig. 2 A programme-controlled furnace in the 2000 kN LOS testing machine

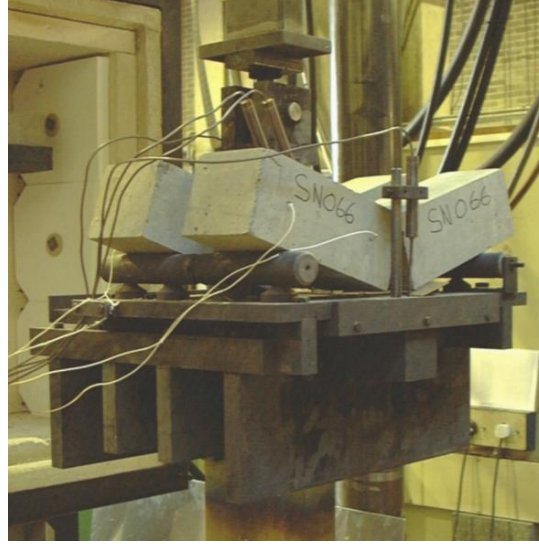


Fig. 3 N-type thermocouples embedded in the beam specimens

Table 3 Fracture properties of the HPC and weight loss for various heating temperatures

$T_m$ (°C)	$f_{cu}$ (MPa)	$f_t'$ (MPa)	$E$ (GPa)	$f_r$ (MPa)	$G_F$ (N/m)	$K_{IC}$ MN/m <sup>1.5</sup>	$K_{IC}'$ MN/m <sup>1.5</sup>	$\omega$ (%)				
State	Cold	Cold	Cold	Hot	Cold	Hot	Cold	Hot	Cold	Hot	Cold	Cold
20	67.1	4.47	35.64	6.35	228.2	1.389	2.845	0.00				
105	55.2	3.40	29.82	4.89	6.43	205.6	223.0	1.101	1.323	2.471	2.574	2.46
150	61.9	3.61	27.05	6.13	6.65	191.5	258.9	1.243	1.316	2.272	2.645	4.59
200	63.7	3.55	23.80	6.33	6.35	212.2	286.4	1.223	1.227	2.247	2.607	5.16
250	62.9	3.31	21.12	6.20	5.92	236.3	310.7	1.164	1.126	2.233	2.558	5.58
300	60.9	3.11	17.57	6.01	5.37	258.6	323.7	1.081	0.996	2.122	2.384	5.97
350	58.8	2.91	14.75	5.81	5.13	273.7	310.1	1.006	0.919	2.007	2.138	6.28
400	56.4	2.71	12.53	5.61	4.87	289.9	280.7	0.939	0.847	1.903	1.869	6.62
450	53.8	2.48	9.99	5.41	4.65	303.2	253.4	0.866	0.771	1.737	1.584	6.76

A 10 kN high temperature load cell, located outside the furnace, was inserted between the top piece and top actuator for load measurement due to its temperature working limit of 180°C and continuously cooled during the heating-testing process so that the actual temperature in the load cell was below 50°C. The displacement of the machine was automatically recorded using a built-in displacement transducer. Four LIN high temperature linear voltage displacement transducers (LVDTs) with a temperature working limit of 600°C were also used for monitoring the creep of the concrete during heating, two for each beam.

Three-point bending tests at high temperatures and after cooling were conducted at a displacement rate of  $1.25 \times 10^{-3}$  mm/s. The load and displacements were recorded using a data

logger at a rate of two sets per second. Each three-point bending test took 10 to 15 minutes.

To monitor the temperature developments in the concrete, N-type thermocouples were embedded in the beams for three-point bending tests. Two positions were chosen for each beam: 50 mm close to the edge (side hole) and 50 mm away from the centre (middle hole) to avoid disturbing the notched mid-section. The 50 mm deep holes were drilled before the beams were heated. The temperatures from the thermocouples in the three heating zones and from the master thermocouple of the furnace were recorded.

The DNG7229 3000 kN machine was used to measure  $f_{cu}$  and  $f_t'$  on at least six cubes for each scenario. The Testwell TE6000 3000 kN servo testing machine was used to test  $E$  on four prisms. All the test results of the fracture characteristics of the concrete for various heating temperatures and test conditions are listed in Table 3.

### 3.3 Weight loss measurement

To continuously monitor the moisture migration during heating, exposure, testing and cooling, two steel cradles were made for hanging concrete beams and prisms, each connected to a VC8000 high precision load cell of  $25 \text{ kg} \pm 10 \text{ g}$ , fixed outside the furnace. During heating, exposure and cooling, the weight changes were recorded every 5 seconds. During testing, the weight changes were recorded together with the load and displacements at a rate of two sets per second. The values of the final weight loss after the cooling-down stage are also included in Table 3.

## 4. Fracture toughness $K_{IC}$ and $K_{IC}'$

### 4.1 Summary of the previous study

The effects of the heating temperature on the fracture energy and other mechanical properties of the high performance concrete at high temperatures up to  $450^\circ\text{C}$  under the hot and cold conditions were reported in the previous publications (Zhang and Bićanić 2006, Zhang 2011). The main findings are summarised as follows.

The measurements using thermocouples indicated that the temperature in the concrete always developed behind the furnace temperature but a thermal equilibrium could be reached if the exposure time was long enough.

The weight loss monotonically increased with the increasing heating temperature. High heating temperatures always led to large weight losses but a hygric equilibrium state could be reached if the exposure time was long enough, in particular for low heating temperatures, e.g. 16 hours for obtaining a hygric equilibrium state in this study.

The fracture energy generally sustained a decrease-increase tendency with the heating temperature for the hot concrete but a hold-increase-decrease tendency for the cold concrete. The fracture energy changed with the ultimate weight loss in a similar way. At the first stage, the evaporation of capillary water at low heating temperatures only slightly affected the fracture energy but the later evaporation of the gel water and chemically combined water and decomposition significantly reduced the fracture energy.

The modulus of rupture decreased with the increasing heating temperature for the hot concrete, but sustained an increase-decrease tendency for the cold concrete. There was a sudden drop at  $105^\circ\text{C}$  for the hot concrete due to high vapour pressure inside the concrete. There existed a tri-

linear decrease-recovery-decrease trend between the modulus of rupture and the ultimate weight loss for the hot concrete and a bi-linear increase-decrease trend for the cold concrete.

The residual compressive and tensile strengths both decreased with the increasing heating temperature. There was a sudden drop in the concrete strengths between 105°C and 150°C due to the residual stress caused by the high vapour pressure inside the concrete. The tensile strength decreased more rapidly than the compressive strength for the same heating scenario. The concrete strengths had two-stage decrease tendencies related to the ultimate weight loss.

The residual Young's modulus of concrete monotonically decreased with the increasing heating temperature and this could be expressed by using a linear relationship. There existed a two-stage linear relationship between the residual Young's modulus and the ultimate weight loss.

#### 4.2 $K_{IC}$ and $K_{IC}'$ versus $T_m$

Fig. 4 shows  $K_{IC}$  and  $K_{IC}'$  for various heating temperatures and testing conditions. In general, both  $K_{IC}$  and  $K_{IC}'$  decreased with the increasing hearing temperature but followed different tendencies.

For the hot concrete,  $K_{IC}$  sustained a decrease-recovery-decrease tendency but generally followed a decreasing tendency with increasing  $T_m$ .  $K_{IC}$  decreased from 1.389 MN/m<sup>1.5</sup> at 20°C to 1.101 MN/m<sup>1.5</sup> at 105°C with a sudden drop of 21%, due to high vapour pressures inside the concrete, but recovered to 1.243 MN/m<sup>1.5</sup> at 150°C. It then continuously decreased to 1.223 MN/m<sup>1.5</sup> at 200°C, 1.081 MN/m<sup>1.5</sup> at 300°C and 0.866 MN/m<sup>1.5</sup> at 450°C with a net drop of 38%.

For the cold concrete,  $K_{IC}$  first decreased slowly with  $T_m$ . At 150°C,  $K_{IC}$  only slightly decreased from 1.389 MN/m<sup>1.5</sup> at 20°C to 1.316 MN/m<sup>1.5</sup>, down by 0.073 MN/m<sup>1.5</sup> or 5%. Thereafter it more rapidly decreased with  $T_m$ , down to 1.227 MN/m<sup>1.5</sup> at 200°C and 0.996 MN/m<sup>1.5</sup> at 300°C. At 450°C,  $K_{IC}$  decreased to 0.771 MN/m<sup>1.5</sup>, with a net drop of 0.618 MN/m<sup>1.5</sup> or 45% which was larger than that for the hot concrete. This means that cooling would cause further damage to the concrete by forming more micro-cracks.

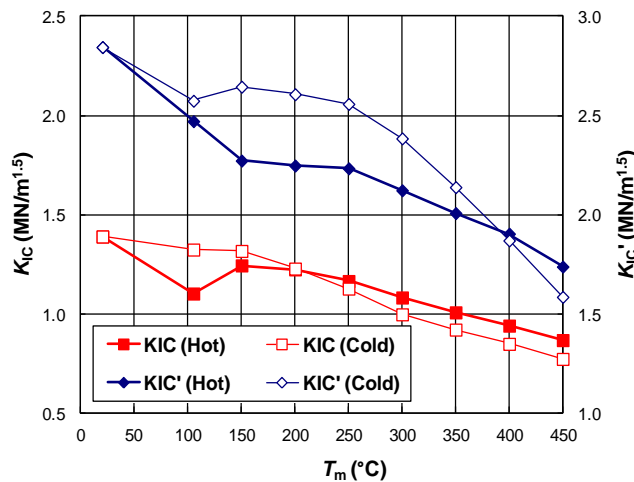


Fig. 4  $K_{IC}$  and  $K_{IC}'$  for different heating temperatures and testing conditions

Fig. 4 also shows that for  $T_m \leq 200^\circ\text{C}$ , the values of  $K_{IC}$  for the hot concrete were smaller than those for the cold concrete. At this stage, the high vapour pressure under the hot conditions could not efficiently evaporate so as to significantly reduce the fracture toughness of the concrete. The cooling process eliminated the vapour pressure and did not damage the concrete. For higher heating temperatures over  $200^\circ\text{C}$ , the values of  $K_{IC}$  for the hot concrete were larger than those for the cold concrete. At this stage, there were no longer high vapour pressures within the concrete because micro cracks had already formed. However, cooling would cause more micro cracks and further damage the concrete. Thus, even smaller fracture toughness would be expected.

From Fig. 4, it can be seen that the values of  $K_{IC}'$  were twice as large as the values  $K_{IC}$  for all heating temperatures and different testing conditions. This is because  $K_{IC}$  is an instantaneous parameter and represents the cracking resistance at the peak load, while  $K_{IC}'$  is a more synthetic process parameter and represents the resistance over the whole fracture process.

For the hot concrete,  $K_{IC}'$  sustained a decrease-hold-decrease tendency but generally followed a decreasing tendency with the increasing  $T_m$ .  $K_{IC}'$  decreased from  $2.845 \text{ MN/m}^{1.5}$  at  $20^\circ\text{C}$  to  $2.272 \text{ MN/m}^{1.5}$  at  $105^\circ\text{C}$ , but was almost unchanged until  $250^\circ\text{C}$  with a value of  $2.233 \text{ MN/m}^{1.5}$ . Thereafter it continuously decreased to  $2.122 \text{ MN/m}^{1.5}$  at  $300^\circ\text{C}$  and  $1.737 \text{ MN/m}^{1.5}$  at  $450^\circ\text{C}$  with a net drop of 39%.

For the cold concrete,  $K_{IC}'$  has a sudden drop at  $105^\circ\text{C}$  from  $2.845 \text{ MN/m}^{1.5}$  at  $20^\circ\text{C}$  to  $2.574 \text{ MN/m}^{1.5}$ , down by  $0.271 \text{ MN/m}^{1.5}$  or 10%. It recovered to  $2.645 \text{ MN/m}^{1.5}$  at  $150^\circ\text{C}$  and then slowly decreased until  $250^\circ\text{C}$  with a value of  $2.558 \text{ MN/m}^{1.5}$ . Thereafter,  $K_{IC}'$  continuously decreased at a higher rate to  $2.138 \text{ MN/m}^{1.5}$  at  $350^\circ\text{C}$  and  $1.584 \text{ MN/m}^{1.5}$  at  $450^\circ\text{C}$ , with a net drop of  $1.261 \text{ MN/m}^{1.5}$  or 44%. For most heating temperatures, the values of  $K_{IC}'$  for the hot concrete were always smaller than those for the cold concrete except for  $T_m \geq 400^\circ\text{C}$ .

#### 4.3 $K_{IC}$ and $K_{IC}'$ versus $\omega$

Fig. 5 shows the relationships of  $K_{IC}$  and  $K_{IC}'$  with the weight loss  $\omega$  for the hot and cold testing conditions. In general, both  $K_{IC}$  and  $K_{IC}'$  decreased with the increasing hearing temperature but followed different tendencies.

For the hot concrete,  $K_{IC}$  had a decrease-recovery-decrease tendency with  $\omega_u$ .  $K_{IC}$  sharply decreased with  $\omega_u$  first from  $1.389 \text{ MN/m}^{1.5}$  at  $20^\circ\text{C}$  to  $1.101 \text{ MN/m}^{1.5}$  at  $105^\circ\text{C}$  with a toughness loss of 21%, corresponding to a threshold weight loss  $\omega_{u1} = 2.46\%$ . At the second stage,  $K_{IC}$  quickly recovered to  $1.243 \text{ MN/m}^{1.5}$  at  $150^\circ\text{C}$  with  $\omega_{u2} = 4.59\%$ . Thereafter,  $K_{IC}$  continuously decreased with  $\omega_u$  again. This tendency can be expressed using a tri-linear relationship. For the cold concrete,  $K_{IC}$  sustained a two-stage slow decrease - fast decrease tendency with  $\omega_u$ . It slightly decreased with  $\omega_u$  until  $150^\circ\text{C}$  with  $\omega_{u2} = 4.59\%$  and then continuously decreased with  $\omega_u$ . A bi-linear  $K_{IC} - \omega_u$  relationship can be used for the cold concrete. Similarly, for  $\omega \leq \omega_{u3} = 5.16\%$  corresponding to  $T_m \leq 200^\circ\text{C}$ , the values of  $K_{IC}$  for the hot concrete were smaller than those for the cold concrete. For higher weight loss over  $\omega_{u3} = 5.16\%$  or higher heating temperatures over  $200^\circ\text{C}$ , the values of  $K_{IC}$  for the hot concrete were larger than those for the cold concrete.

Also for the hot concrete,  $K_{IC}'$  had a slow decrease - fast decrease tendency with  $\omega_u$ .  $K_{IC}'$  continuously but slowly decreased with  $\omega_u$  first from  $2.845 \text{ MN/m}^{1.5}$  at  $20^\circ\text{C}$  to  $2.233 \text{ MN/m}^{1.5}$  at  $250^\circ\text{C}$  with a toughness loss of 22%, corresponding to a threshold weight loss  $\omega_{u4} = 5.58\%$ . At the second stage,  $K_{IC}'$  continuously but quickly decreased with  $\omega_u$ . This tendency can be expressed using a bi-linear relationship. For the cold concrete,  $K_{IC}'$  sustained a three-stage decrease-hold-decrease tendency with  $\omega_u$ . It slightly decreased with  $\omega_u$  until  $105^\circ\text{C}$  with  $\omega_{u1} = 2.46\%$  and then

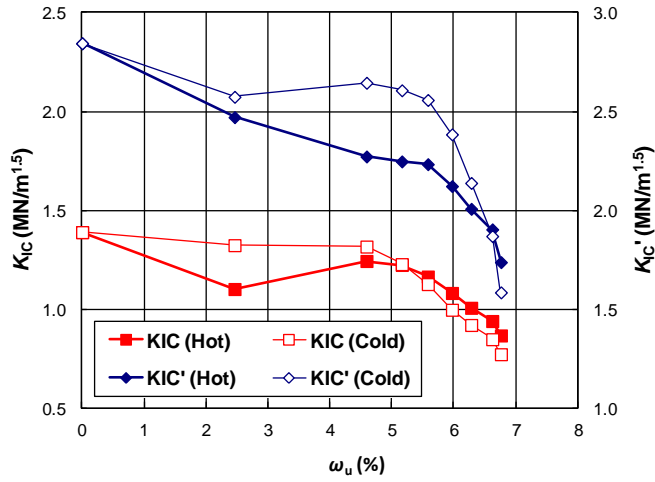


Fig. 5  $K_{IC}$  and  $K_{IC}'$  versus ultimate weight loss  $\omega_u$

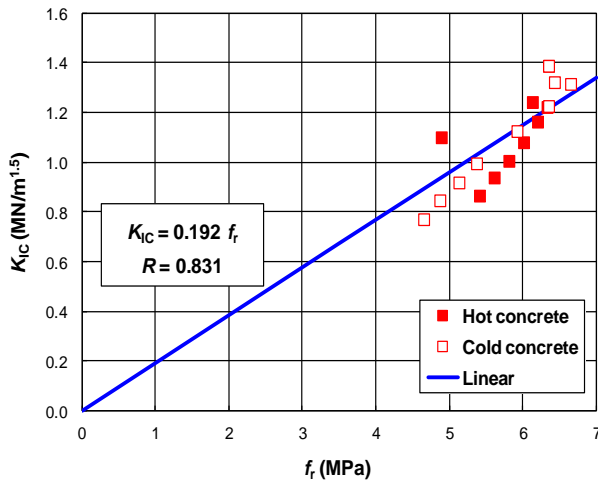


Fig. 6 Relationship between  $K_{IC}$  and  $f_r$  for different heating temperatures

was almost unchanged until  $\omega_{u4} = 5.58\%$  corresponding to  $250^\circ\text{C}$ . Thereafter  $K_{IC}'$  rapidly decreased with  $\omega_u$ . A tri-linear  $K_{IC}' - \omega_u$  relationship can be used for expressing the trend for the cold concrete. Similarly, for  $\omega \leq \omega_{u5} = 6.62\%$  corresponding to  $T_m \leq 400^\circ\text{C}$ , the values of  $K_{IC}'$  for the hot concrete were smaller than those for the cold concrete. For higher weight loss over  $\omega_{u5} = 6.62\%$  or higher heating temperatures over  $400^\circ\text{C}$ , the values of  $K_{IC}'$  for the hot concrete were larger than those for the cold concrete.

#### 4.4 $K_{IC}$ versus $f_r$

Fig. 6 illustrates a relationship between  $K_{IC}$  and  $f_r$  for all the heating temperatures and testing conditions. It can be seen that all the test results can be represented by a linear equation as

$$K_{IC} = 0.192 f_r \quad \text{or} \quad K_{IC} = 0.768 \sigma_N \quad (9)$$

with a linear correlation coefficient  $R = 0.831$ . This relationship can also be directly confirmed from Eq. (1). In comparison with Eq. (1), the term  $\sqrt{a} F(\alpha)$  can be obtained as 0.768. This means that for a given material and geometry, the classic fracture toughness  $K_{IC}$  can be fully determined by the modulus of rupture of the notched beam. In this study, however, the correlation between the fracture toughness  $K_{IC}$  and the modulus of rupture  $f_r$  is not as good as that reported in the previous study on the residual fracture properties of the normal- and high-strength concrete subjected to high temperatures by the first author (Zhang and Bićanić 2002a). This is because the majority of  $f_r$  values fell within 4.0 to 7.0 MPa rather than largely distributed even though  $K_{IC}$  varied largely with the heating scenarios.

## 5. Conclusions

In this study, the fracture toughness  $K_{IC}$  of high performance concrete, together with the fracture energy related fracture toughness  $K_{IC}'$ , was evaluated by conducting three-point bending tests on eighty notched beams at high temperatures up to 450°C (hot) and in slow cooled-down states (cold). The exposure time was maintained as 16 hours, and both thermal and hygric equilibriums were achieved. The weight loss  $\omega$  was continuously monitored during the complete heating, exposure, testing and cooling process. The following conclusions can be drawn accordingly.

- $K_{IC}$  for the hot concrete sustained a monotonic decrease tendency with the heating temperature, with a sudden drop at 105°C. For the cold concrete,  $K_{IC}$  sustained a two-stage decrease trend, dropping slowly with the heating temperature up to 150°C and rapidly thereafter. When  $T_m \leq 200^\circ\text{C}$ ,  $K_{IC}$  for the hot concrete was smaller than that for the cold concrete, and a reverse trend occurred for higher heating temperatures.
- $K_{IC}'$  was twice as large as  $K_{IC}$  for all heating temperatures because  $K_{IC}$  is an instantaneous parameter and represents the cracking resistance at the peak load, while  $K_{IC}'$  is a more synthetic process parameter and represents the resistance over the whole fracture process.
- For both hot and cold concrete,  $K_{IC}'$  sustained a decrease-hold-decrease tendency with  $T_m$ . For most heating temperatures,  $K_{IC}'$  for the hot concrete was always smaller than that for the cold concrete except for  $T_m \geq 400^\circ\text{C}$ .
- For the hot concrete,  $K_{IC}$  sustained a decrease-recovery-decrease tendency with the final weight loss  $\omega_u$ . In the first two stages,  $K_{IC}$  only slightly decreased with  $\omega_u$  until 150°C and then dropped rapidly.  $K_{IC}$  for the cold concrete clearly followed a two stage decrease trends, dropping slowly with  $\omega_u$  first and then rapidly after 150°C.
- For the hot concrete,  $K_{IC}'$  sustained a two stage decrease tendency with  $\omega_u$ .  $K_{IC}'$  first slowly decreased with  $\omega_u$  until 250°C. At the second stage,  $K_{IC}'$  continuously but quickly decreased with  $\omega_u$ . For the cold concrete,  $K_{IC}'$  sustained a three-stage decrease-hold-decrease tendency with  $\omega_u$ . It slightly decreased with  $\omega_u$  until 105°C and then was almost unchanged until 250°C. Thereafter  $K_{IC}'$  rapidly decreased with  $\omega_u$ .
- A fairly linear relationship between  $K_{IC}$  and  $f_r$  existed for the test results in this study.

## Acknowledgments

This project was conducted under the British Energy contract PP/120543/DGD/HN.

## References

- Abe, T., Furumura, F., Tomatsuri, K., Kuroha, K. and Kokubo, I. (1999), "Mechanical properties of high strength concrete at high temperatures", *J. Struct. Construct. Eng.*, **515**, 163-168.
- Baker, G. (1996), "The effect of exposure to elevated temperatures on the fracture energy of plain concrete", *RILEM Mater. Struct.*, **29**, 383-388.
- Bangi, M.R. and Horiguchi, T. (2011), "Pore pressure development in hybrid fibre-reinforced high strength concrete at elevated temperatures", *Cement Concrete Res.*, **41**, 1150-1156.
- Bazant, Z.P. and Oh, B.H. (1983), "Crack band theory for fracture of concrete", *RILEM Mater. Struct.*, **16**(93), 155-177.
- Bazant, Z.P. (1984), "Size effect in blunt fracture: concrete rock and metal", *ASCE J. Eng. Mech.*, **110**(4), 518-535.
- Bazant, Z.P., Kim, J.K. and Pfeiffer, P.A. (1986), "Nonlinear fracture properties from size effect tests", *ASCE J. Struct. Eng.*, **112**(2), 289-307.
- Bazant, Z.P. and Prat, P.C. (1988), "Effect of temperature and humidity on fracture energy of concrete", *ACI Mater. J.*, **85**(4), 262-271.
- Bazant, Z.P. and Kaplan, M.F. (1996), *Concrete at High Temperatures: Material Properties and Mathematical Models*, Longman Group Limited, Harlow Essex, England.
- Chen, B. and Liu, J. (2004), "Residual strength of hybrid-fiber-reinforced high-strength concrete after exposure to high temperatures", *Cement Concrete Res.*, **34**, 1065-1069.
- Cülfik, M.S. and Özturan, T. (2002), "Effect of elevated temperatures on the residual mechanical properties of high-performance mortar", *Cement Concrete Res.*, **32**, 809-816.
- Elices, M., Guinea, G.V. and Planas, J. (1992), "Measurement of the fracture energy using three-point bend tests: part 3 — influence of cutting the P- $\delta$  tail", *RILEM Mater. Struct.*, **25**, 137-163.
- Felicetti, R. and Gambarova, P.G. (1998), "Effects of high temperatures on the residual compressive strength of high-strength siliceous concretes", *ACI Mater. J.*, **95**(4), 395-406.
- Gettu, R., Bazant, Z.P. and Karr, M.E. (1990), "Fracture properties and brittleness of high-strength concrete", *ACI Mater. J.*, **87**(6), 608-618.
- Guinea, G.V., Planas, J. and Elices, M. (1992), "Measurement of the fracture energy using three-point bend tests: part 1 — influence of experimental procedures", *RILEM Mater. Struct.*, **25**, 212-218.
- Haghighi, A., Koohkan, M.R. and Shekarchizadeh, M. (2007), "Optimising concrete using group method of data handling and genetic programme", *32<sup>nd</sup> Conference on Our World in Concrete and Structures*, Singapore.
- Hamoush, S.A., Abdel-Fattah, H. and McGinley, M.W. (1998), "Residual fracture toughness of concrete exposed to elevated temperature", *ACI Materials J.*, **95**(6), 689-694.
- Hillerborg, A., Modeer, M. and Petersson, P.E. (1976), "Analysis of crack formation and crack growth in concrete by means of fracture mechanics and finite elements", *Cement Concrete Res.*, **6**(6), 773-782.
- Ince, R. (2010), "Determination of concrete fracture parameters based on two-parameter and size effect models using split-tension cubes", *Eng. Fract. Mech.*, **77**, 2233-2250.
- Kanellopoulos, A., Farhat, F.A., Nicolaidis, D. and Karihaloo, B.L. (2009), "Effect of elevated temperatures on the residual mechanical properties of high-performance mortar", *Cement Concrete Res.*, **39**, 1087-1094.
- Kaplan, M.F. (1961), "Crack propagation and the fracture of concrete", *ACI J.*, **58**(5), 591-610.
- Karihaloo, B.L. and Nallathambi, P. (1989), "An improved effective crack model for the determination of fracture toughness of concrete", *Cement Concrete Res.*, **19**, 603-610.

- Karihaloo, B.L., Murthy, A.R. and Iyer, N.R. (2013), "Determination of size-independent specific fracture energy of concrete mixes by the tri-linear model", *Cement Concrete Res.*, **49**, 82-88.
- Kwon, S.H., Zhao, Z. and Shah, S.P. (2008), "Effect of specimen size on fracture energy and softening curve of concrete: Part II. Inverse analysis and softening curve", *Cement Concrete Res.*, **38**, 1061-1069.
- Murthy, A.R., Karihaloo, B.L., Iyer, N.R., and Raghu Prasad, B.K. (2013), "Determination of size-independent specific fracture energy of concrete mixes by the two methods", *Cement Concrete Res.*, **50**, 19-25.
- Nallathambi, P., Karihaloo, B.L. and Heaton, B.S. (1984), "Effect of specimen and crack sizes, water/cement ratio and coarse aggregate texture upon fracture toughness of concrete", *M. Concrete Res.*, **36**(129), 227-236.
- Nielsen, C.V. (1995), "Ultra high-strength steel fibre reinforced concrete, Part I Basic strength properties of compresit matrix", Ph.D. Dissertation, Department of Structural Engineering, Technical University of Denmark, Denmark.
- Nielsen, C.V. and Bićanić, N. (2003), "Residual fracture energy of high-performance and normal concrete subject to high temperatures", *RILEM Mater. Struct.*, **36**(8), 515-521.
- Peng, G.F., Yang, W.W., Zhao, J., Liu, Y.F., Bian, S.H. and Zhao, L.H. (2006), "Explosive spalling and residual mechanical properties of fiber-toughened high-performance concrete subjected to high temperatures", *Cement Concrete Res.*, **36**, 723-727.
- Phan, L.T. and Carino, N.J. (1998), "Review of mechanical properties of HSC at elevated temperature", *ASCE J. Mater. Civil Eng.*, **10**(1), 58-64.
- Phillips, D.V. and Zhang, B. (1993), "Direct tension tests on notched and un-notched plain concrete specimens", *M. Concrete Res.*, **45**, 25-35.
- Planas, J., Elices, M. and Guinea, G.V. (1992), "Measurement of the fracture energy using three-point bend tests: part 2 — influence of bulk energy dissipation", *RILEM Mater. Struct.*, **25**, 305-312.
- Prokoski, G. (1995), "Fracture toughness of concrete at high temperature", *J. Mater. Sci.*, **30**, 1609-1612.
- Pu, X. (2012), *Super-High-Strength High Performance Concrete*, CRC Press.
- RILEM Technical Committee 50 FMC (1985), "Draft recommendation: determination of the fracture energy of mortar and concrete by means of three-point bend test on notched beams", *RILEM Mater. Struct.*, **18**(106), 285-290.
- RILEM Technical Committee 89 FME (1990a), "Draft recommendation: determination of fracture parameters ( $K_{IC}^S$  and CTOD<sub>c</sub>) of plain concrete using three-point bend tests", *RILEM Mater. Struct.*, **23**, 457-460.
- RILEM Technical Committee 89 FME (1990b), "Draft recommendation: size-effect method for determining fracture energy and process zone size of concrete", *RILEM Mater. Struct.*, **23**, 461-465.
- Rosselló, C. and Elices, M. (2004), "Fracture of model concrete 1. Types of fracture and crack path", *Cement Concrete Res.*, **34**, 1441-1450.
- Rosselló, C., Elices, M. and Guinea, G.V. (2006), "Fracture of model concrete: 2. Fracture energy and characteristic length", *Cement Concrete Res.*, **36**, 1345-1353.
- Schneider, U. (1988), "Concrete at high temperatures - a general review", *Fire Safety J.*, **13**, 55-68.
- Shah, S.P. (1990), "Experimental methods for determining fracture process zone and fracture parameters", *Eng. Fract. Mech.*, **35**(1/2/3), 3-14.
- Ulm, F.-J. and James, S. (2011), "The scratch test for strength and fracture toughness determination of oil well cements cured at high temperature and pressure", *Cement Concrete Res.*, **41**, 942-946.
- Watanabe, K., Bangi, M.R. and Horiguchi, T. (2013), "The effect of testing conditions (hot and residual) on fracture toughness of fiber reinforced high-strength concrete subjected to high temperatures", *Cement Concrete Res.*, **51**, 6-13.
- Xu, S. and Reinhardt, H.W. (1999a), "Determination of double-K criterion for crack propagation in quasi-brittle materials. Part I: Experimental investigation of crack propagation", *Inter. J. Fract.*, **98**, 111-149.
- Xu, S. and Reinhardt, H.W. (1999b), "Determination of double-K criterion for crack propagation in quasi-brittle materials. Part II: Analytical evaluating and practical measuring methods for three-point bending

- notched beams”, *Inter. J. Fract.*, **98**, 151-77.
- Xu, S. and Reinhardt, H.W. (1999), “Determination of double-K criterion for crack propagation in quasi-brittle materials. Part III: Compact tension specimens and wedge splitting specimens”, *Int. J. Fract.*, **98**, 179-193.
- Xu, S. and Reinhardt, H.W. (2000), “A simplified method for determining double-K fracture parameters for three-point bending tests”, *Inter. J. Fract.*, **104**, 181-209.
- Yan, Y.N., Luo, X. and Sun, W. (2000), “Compressive strength and pore structure of high-performance concrete after exposure to high temperature up to 800°C”, *Cement Concrete Res.*, **30**, 247-251.
- Yu, K. and Lu, Z. (2013), “Determining residual double-K fracture toughness of post-fire concrete using analytical and weight function method”, *Mater. Struct.*, Published on line on 23 May 2013.
- Zhang, B., Bićanić, N., Pearce, C.J. and Balabanic, G. (2000a), “Residual fracture properties of normal- and high-strength concrete subject to elevated temperatures”, *M. Concrete Res.*, **52**(2), 123-136.
- Zhang, B., Bićanić, N., Pearce, C.J. and Balabanic, G. (2000b), “Assessment of toughness of concrete subjected to elevated temperatures from complete load-displacement curve — Part I: General introduction”, *ACI Mater. J.*, **97**(5), 550-555.
- Zhang, B., Bićanić, N., Pearce, C.J. and Balabanic, G. (2000c), “Assessment of toughness of concrete subjected to elevated temperatures from complete load-displacement curve — Part II: Experimental investigations”, *ACI Mater. J.*, **97**(5), 556-566.
- Zhang, B. and Bićanić, N. (2002a), “Residual fracture toughness of normal- and high-strength gravel concrete after heating to 600°C”, *ACI Mater. J.*, **99**(3), 217-226.
- Zhang, B., Bićanić, N., Pearce, C.J. and Phillips, D.V. (2002b), “Relationship between brittleness and moisture loss of concrete exposed to high temperatures”, *Cement Concrete Res.*, **32**, 363-371.
- Zhang, B. and Bićanić, N. (2006), “Fracture energy of high-performance concrete at high temperatures up to 450°C: the effects of heating temperatures and testing conditions (hot and cold)”, *M. Concrete Res.*, **58**(5), 277-288.
- Zhang, B. (2011), “Effects of moisture evaporation (weight loss) on fracture properties of high performance concrete subjected to high temperatures”, *Fire Safety J.*, **46**, 543-549.
- Zhang, B., Cullen, M. and Kilpatrick, T. (2013), “Effects of thermal and hygric gradients on the spalling of high performance concrete subjected to elevated temperatures”, *The 2013 International Conference on Computational Technologies in Concrete Structures*, 8-12 September 2013, Jeju, Korea.
- Zhao, Z., Kwon, S.H. and Shah, S.P. (2008), “Effect of specimen size on fracture energy and softening curve of concrete: Part I. Experiments and fracture energy”, *Cement Concrete Res.*, **38**, 1049-1060.